NTNU – Trondheim
Norwegian University of
Science and Technology

Comparing an Analytical Cascade Spectrum of High Energy Gamma Rays to those found in a Monte Carlo simulation

Martin Bromstad Skrove

Physics
Submission date: June 2014
Supervisor: Michael Kachelriess, IFY

Norwegian University of Science and Technology
Department of Physics

"Though no one can go back and make a brand new start, anyone can start from now and make a brand new ending."

Carl Bard

NORWEGIAN UNIVERSITY OF SCIENCE AND TECHNOLOGY

Abstract

Department of Physics

Master of Science in Physics

Comparing an Analytical Cascade Spectrum of High Energy Gamma Rays to those found in a Monte Carlo simulation

by Martin Skrove

In this thesis we consider the analytical model for electromagnetic cascades initiated by very high energy gamma rays due to Berezinskii et. al [1]. We compare the analytical prediction that the spectral energy distribution is described in general terms by a broken power-law, to findings made using a Monte Carlo simulation of such electromagnetic cascades. Our findings are that the analytical model predicts the general energy dependence of the cascade spectrum very well, and that it is remarkably insensitive to the source parameters.

Acknowledgements

I would like to thank my supervisor, Prof. Michael Kachelrieß, whose great knowledge, genuine interest and legendary patience has been indispensable.

This thesis is dedicated to my father, to whom I would have had to explain everything in great detail, several times over, and at a great expense of my patience. I miss doing so very much.

Contents

List of Figures

Chapter 1

Introduction

High energy gamma rays are important to the study of astrophysical objects that act as both gamma ray sources and cosmic ray sources. The acceleration of cosmic rays has been an open question in physics for the better part of a century, and while we now have good candidate theories to resolve this question the acceleration of cosmic rays at the very highest energies are still an open question. Such ultra high energy cosmic rays (UHECR) are thought to be extragalactic in origin because there are no known astrophysical objects close to us who might theoretically support their acceleration. One of the most interesting potential sources of UHECRs are a class of Active Galactic Nuclei (AGN) which are known as blazars. Blazars are AGNs where the relativistc jet is pointed towards Earth, meaning they are incredibly luminous objects on the sky. The problem with the direct study of cosmic rays is that they are deflected by the extragalactic magnetic field (EGMF), which seemingly exists throughout the entire large scale structure of the universe. However, AGNs are also thought to be strong gamma ray sources and unlike the charged cosmic rays, neutral gamma rays propagate freely through magnetic fields.

Gamma ray sources are still not entirely freed from the influence of the EGMF. Very high energy gamma rays can interact with background photons through the pair production interaction $\gamma_{HE} + \gamma_b \rightarrow e^+ + e^-$. If the initial gamma ray was energetic enough, both the electron and positron produced can transfer their energy on to additional background photons through inverse Compton scattering $e + \gamma_b \rightarrow \gamma_{HE} + e'$. If the initial gamma ray was of particularly high energy, this process can carry on and results in a single VHE gamma ray producing a multitude of high energy photons. This process is called an electromagnetic cascade. Incidentally, this also has the effect of connecting the gamma ray flux to the EGMF

since the charged component of the cascade[1] can be deflected. Furthermore, the cascade is dependent on the presence of background photons in order to initiate and evolve. The universe is populated by a series of photon populations, the major of which are the cosmic microwave background (CMB) as well as the extragalactic background light (EBL). The CMB is well established to be residual thermal radiation from the big bang, while the EBL[2] is the sum of the diffuse starlight from galaxies as well as re-emittance of some absorbed portion of this from space dust. Thus, since the formation and development of an electromagnetic cascade depends on the EBL, and since the charged component which arises through such a cascade makes the resulting gamma ray spectrum sensitive to the EGMF, any attempt to observe gamma ray emissions from some astrophysical source such as for instance a blazar is dependent on knowledge of both the EBL and the EGMF. Therefore, in order to study sources of such very interesting things as UHECRs we need detailed information on the EBL and EGMF, which is hard to come by. This makes answering such questions as the acceleration mechanism of UHECRs a very challenging effort.

High energy astrophysics of cosmic rays and gamma rays is a wide field of research. Ever since the first observation of cosmic rays in 1912 the topic has been diligently pursued. There are several novel methods to determine bounds on the EGMF and a well-written review of the topic is presented by Durrer & Neronov in [19]. Measuring the EBL is very difficult due to its low energy density and the presence of zodiacal light which disturbs measurements. A wide variety of EBL models exist, and the study of different EBL models is now a field of research in its own right [11]. In this paper we will mainly consider the models of Kneiske [15], Kneiske & Dole [16] and of Finke et. al [17]. The study of actual gamma ray spectral energy distributions is best done through detailed Monte Carlo simulations that account for the evolution of the EBL through cosmological epochs and which incorporates the effects of the EGMF. Such simulations can act as a laboratory for high energy physics and through comparison with observations allow us to constrain the allowed ranges of both the EBL and the EGMF. We will consider an analytical model for electromagnetic cascades due to Berezinskii [1], which describes the general features of the energy distribution of the cascade. Our goal is to compare the analytical predictions to those made from a Monte Carlo simulation in order to test the generality of the analytical model for different EBL models, sources and EGMF values.

[1] Electrons and positrons, which we will frequently simply refer to as 'electrons'.

[2] On occasion the term EBL refers only to the diffuse starlight and the dust re-radiation, but sometimes we also mean to include the CMB.

Chapter 2

Cosmic Rays

Earth's atmosphere is continuously bombarded by particles originating from outer space. These particles are often ionized nuclei and most of them have relativistic energies, some even as high as 10^{20} eV. These are what we refer to when we say "Cosmic Rays". We also differentiate between "primary" cosmic rays, those accelerated at astrophysical sources, and "secondaries", those particles produced during interaction between the primaries and the galactic medium. Highly relevant secondaries include gamma rays and neutrinos, which are also discussed here. The natural question to ask is "What is the composition of the cosmic ray spectrum and its energy distribution?" but the real challenge is answering where they come from and, especially for the ultra-high-energy cosmic rays, how they are accelerated to such incredible energies.

2.1 Observations

2.1.1 Composition

The basic quantity to describe cosmic rays is the intensity I. Intensity is defined as the number of particles per unit solid angle that pass per unit time through a unit area perpendicular to the direction of observation, $[I] = \mathrm{cm}^{-2}\mathrm{s}^{-1}\mathrm{sr}^{-1}$. For a particle of species i with corresponding intensity I_i the particle flux becomes $\mathcal{F}_i = \int I_i \cos\theta d\Omega$. Assuming an isotropic intensity the flux from one hemisphere

becomes

$$\mathcal{F}_i = I_i \int_0^{2\pi} d\phi \int_0^{\frac{\pi}{2}} \cos\theta \sin\theta d\theta = \pi I_i, \tag{2.1}$$

and the number density of particles will follow

$$N(v) = \frac{4\pi I_i(E)}{v}. \tag{2.2}$$

Here we introduced the *differential* intensity $I_i(E)$, meaning that $I_i(E)\mathrm{d}E$ is the intensity of particles of type i with energy in the interval $[E, E+\mathrm{d}E]$, emphasizing that cosmic rays do not all have the same energy. The *integral* intensity is equal to

$$I_i(>E) = \int_E^\infty E_i(E)\mathrm{d}E \tag{2.3}$$

and describes the intensity of particles with total energy larger than E. The intensity measured by a detector will in general depend not only on energy, but also on its position ($\vec{x}$) and which way the detector is looking (θ, ϕ), meaning $I = I(\vec{x}, p, \theta, \phi)$. From the definition $I = \mathrm{d}N/(\mathrm{d}E\mathrm{d}t\mathrm{d}A\mathrm{d}\Omega)$ and the phase space distribution function $\mathrm{d}N = f(\vec{x}, \vec{p})\mathrm{d}^3x\mathrm{d}^3p$ we can then relate

$$I(\vec{x}, p, \theta, \phi) = vp^2 \frac{\mathrm{d}p}{\mathrm{d}E} f(\vec{x}, \vec{p}) = p^2 f(\vec{x}, \vec{p}). \tag{2.4}$$

From Figure 2.1 we find that in the energy range from several GeV to ≈ 100 TeV, roughly 79% of all primary nucleons are free protons, with the remaining mostly being bound in helium nuclei. In the given energy range the fractions of primary nuclei are nearly constant and their intensity is well described by an inverse power law

$$I_N(E) \approx 1.8 \times 10^4 (E/1\ \mathrm{GeV})^{-\alpha} \frac{\textbf{nucleons}}{\mathrm{m}^2\ \mathrm{s}\ \mathrm{sr}\ \mathrm{GeV}} \tag{2.5}$$

where E is the energy per nucleon, $\alpha \equiv \gamma + 1 = 2.7$ is the differential spectral index of the cosmic ray flux and γ is the integral spectral index. However, it is possibly to see that the relative contribution of heavy elements increase slightly with energy. In Figure 2.2 we see the combined spectrum of all particle species. At $E = 10^{15}$ eV the slope of the spectrum changes from $\alpha = 2.7$ to about $\alpha = 3.0$, referred to as the "knee", and beyond 10^{18} eV the features of the spectrum changes drastically. This power-law distribution is indicative of a non-thermal production mechanism: We can not introduce a meaningful temperature scale to the spectrum and no conceivable thermal process could accelerate cosmic rays to energies as high as 10^{20} eV.

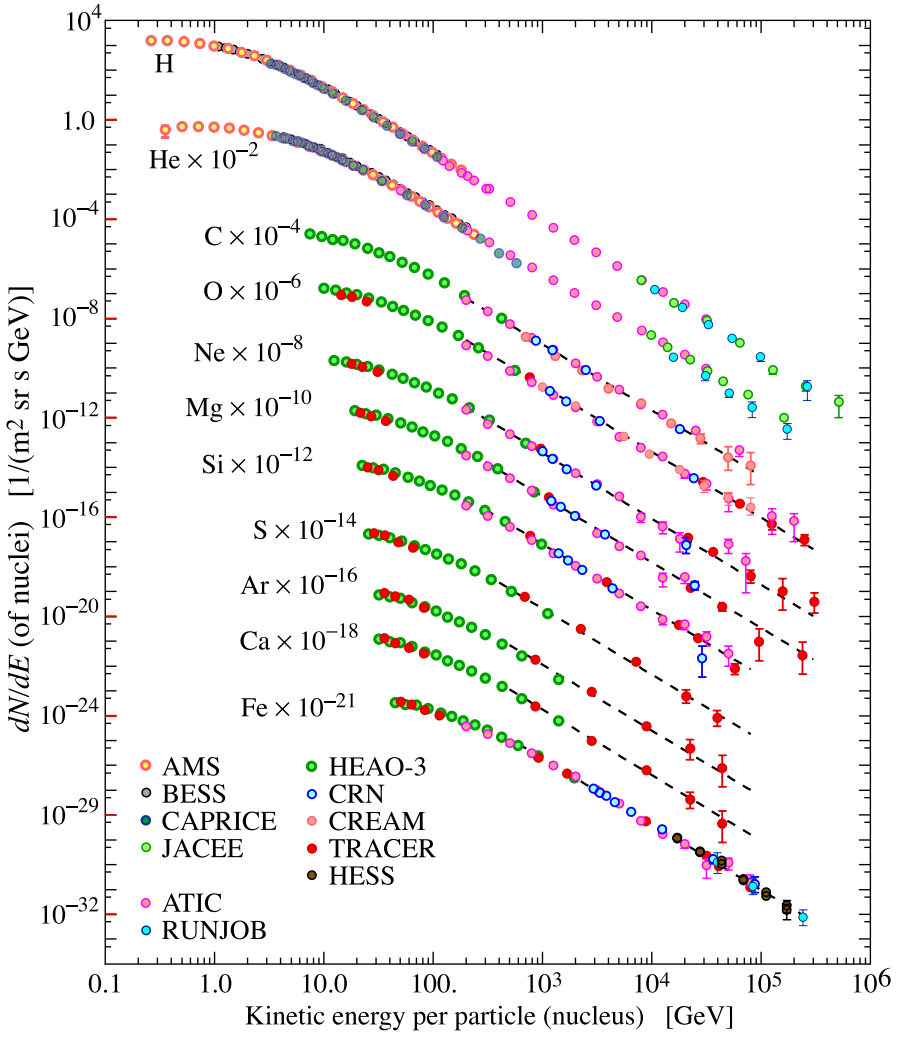

FIGURE 2.1: Primary Cosmic Ray flux of nuclei in units of particles per energy-per-nucleus vs energy per nucleus. [PDG CR Review 2012]

In the mildly relativistic regime of a few GeV per nucleus observation of cosmic rays is relatively easy as fluxes of cosmic rays are high enough to be statistically significant with modest experiments. For decreasing energy the cosmic rays are impaired by solar modulation: The outward flowing solar wind decelerates and partially excludes incoming particles. Additionally comes solar energetic particles and anomalous cosmic rays which contribute as "noise". This in part explains the deviation from the power-law for lower energies visible in Figure 2.1. For increasing energies, detection becomes more difficult due to decreased flux and higher technical complexity in experiments. Two particular features in the spectrum emerge. The aforementioned "knee" at $E \approx 10^{15}$ eV could be explained by cosmic

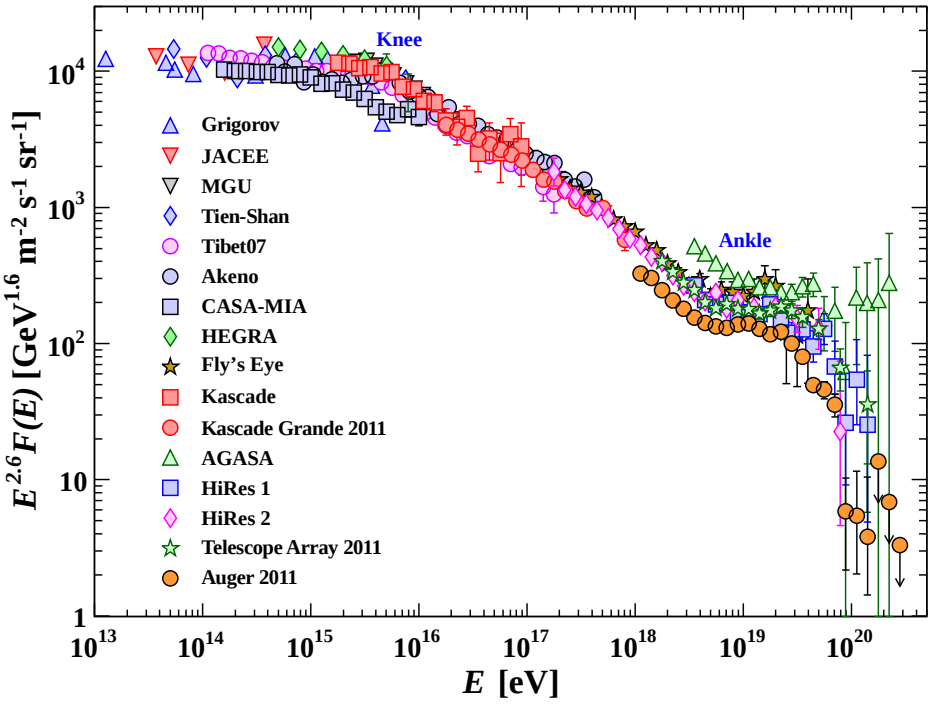

FIGURE 2.2: Combined energy spectrum of cosmic rays in units of particles per energy-per-nucleus vs energy-per-nucleus [PDG CR Review 2012]

ray accelerators in the galaxy reaching their energy limit. For instance, certain types of expanding supernova remnants are thought to be unable to accelerate particles beyond 10^{15} eV. For a full treatment of this feature, galactic propagation and confinement must also be considered. The hardening of the spectrum beyond 10^{18} eV, popularly named the "ankle", can best be explained by the addition of an extragalactic flux which begins to dominate. This suggests an important distinction on the origin of cosmic rays: Galactic vs. Extragalactic.

2.1.1.1 Gamma Rays

Cosmic ray sources will also almost always produce gamma rays. Hadrons accelerated at some source can scatter on gas, producing π^0-mesons which decays rapidly into two photons. Should the source produce high energy electrons these

can produce photons in several ways: bremsstrahlung in the ambient medium, synchrotron radiation in local magnetic fields or through inverse Compton scattering. In all cases, electrons transfer a sizeable portion of their energy to a photon which could emerge as a gamma ray. So while cosmic accelerators are thought to accelerate charged particles, these in turn produce gamma rays as secondary products at the source and in the line-of-sight. The significance of gamma rays is that these are not deflected by magnetic fields in the way charged particles are so the pointing information is not lost. Gamma rays detected on Earth are therefore an important tool in the study of both sources and the effects magnetic fields have on propagation.

2.1.1.2 Other Components

Briefly mentioned as source products were electrons. These are not a large part of the observed spectrum, even though they can be very present at the source, and account for around 1% of the total flux on Earth. In contrast to protons and nuclei, which are far heavier, relativistic electrons lose their energy much more effectively during synchrotron radiation, bremsstrahlung and inverse Compton scattering. The final part of the CR spectrum consists of neutrinos. Several important sources of astrophysical neutrinos exist, and one of them is the production of high energy neutrinos as a result of collisions between charged particles and atomic nuclei or low energy photons. This produces neutrinos through charged pion decay. Neutrinos share with photons the very useful feature of being unaffected by magnetic fields, thus pointing information to the source is not lost. Additionally, neutrinos have tremendous penetrating power due to their negligible interaction rate. While observing neutrinos is challenging, they offer insight into processes where charged particles and photons give limited information due to interactions.

2.2 Origin of Cosmic Rays

The origin of cosmic rays is essentially three questions, we want a theory that describes the origin of particles, the energy and how the particles are accelerated. Initially we follow the presentation of Drury [2].

2.2.1 Origin of Particles

The atomic nuclei that make up the cosmic ray spectrum must originally come from some astrophysical reservoir which we wish to identify. To do so we inspect the composition of nuclei in the spectrum to see if this matches some specific source. More precisely, we compare the abundance of different species at the same energy per nucleon for the relevant energy range. Then we try to find a source that matches this ratio. In the mildly relativistic region where we expect cosmic rays to be of galactic origin this ratio matches the standard Galactic abundance of the interstellar medium (ISM) within first approximation. Notably, the ISM does not contain a significant fraction of nuclei that are not part of any major process in stellar nucleosynthesis, but some elements such as the Li-Be-B group (Z = 3-5) are much more abundant in the CR composition. This can be explained by production of secondary nuclei during CR propagation in the galaxy. Other exceptions exist and have been studied.

2.2.2 Origin of Energy

Cosmic rays that are propagating lose energy through interactions, and for distant sources observed CR energies are also modulated by the cosmological redshift. Models describing the propagation of galactic CRs find that the power needed to sustain the measured CR population in the galaxy is 10^{41} ergs^{-1} [2]. We must then ask what source of energy is sufficient to run an accelerator that produces this kind of output. The only possible energy source of this magnitude is the explosion of supernovae. The energy per supernova is of order 10^{51} erg [4] and they occur averagely every 30 year. This gives a power available in bulk motion of 10^{42} ergs^{-1} which could support the population of CRs provided some acceleration mechanism is found which can reach 10% efficiency. In terms of energy one could favour alternative origins, for instance the radiation luminosity from all the stars in the Galaxy is significantly larger, but there is no known mechanism that allows photons to drive the acceleration of charged particles. For supernovae the decisive feature is that energy is released as kinetic energy.

2.2.3 Sources and Acceleration

Energetically speaking, supernova remnants (SNR) are good candidates for the bulk production of cosmic rays, provided that an acceleration process exists which yields high energy particles obeying a power-law distribution over the required range of energies. In Fermi acceleration charged particles are accelerated through repeated scattering events within a magnetic field. One type of Fermi acceleration which occurs in non-relativistic shock waves is now widely accepted as being capable of accelerating cosmic rays in SNRs. This mechanism is called diffusive shock acceleration (DSA).

2.2.3.1 Diffusive Shock Acceleration

The principle idea behind DSA is that a particle with Larmor radius much larger than the width of the shock can move between the upstream and downstream region of the shock. The Larmor radius of a particle with charge Ze, momentum p, moving in a magnetic field of strength B is

$$R_L = \frac{p}{ZeB} \tag{2.6}$$

and describes the radius of circular motion of the particle in the magnetic field. For each crossing of the shock the particle will gain energy, and after many crossings can be accelerated to very high energies. For this to happen there must be some form of containment close to the shock that keeps the particle bouncing back and forth. The expanding shock front produces turbulence in its wake, and this magnetic turbulence can scatter fast moving charged particles back towards the shock. In the upstream region charged particles attempting to escape the shock will excite Alfvén waves. For a fast moving particle this will look like a magnetic inhomogeneity with which the particle can make numerous small angle scattering events.

To summarize, particles are scattered back and forth from the turbulence downstream of the shock and excited Alfvén waves in the upstream of the shock. The important feature is that these scattering events are elastic so energy is not lost in the process. On the other hand, whenever the particles cross the shock wave they gain energy due to the difference in velocity between the upstream and downstream region. Consider a shock as pictured in Figure 2.3. In the frame of the shock the upstream stellar medium flows towards the shock with a velocity v_u and

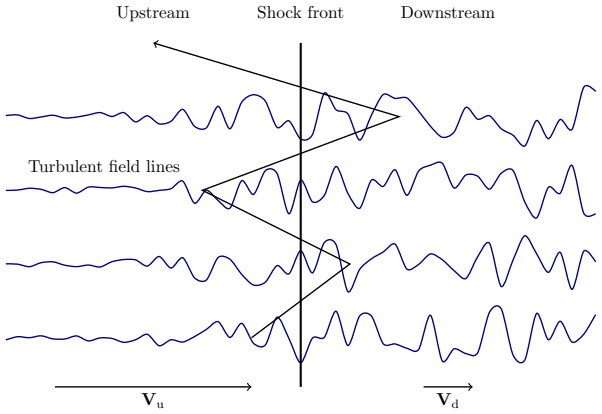

FIGURE 2.3: Diffusive Shock Acceleration in the frame of a fast moving shock, http://sprg.ssl.berkeley.edu/~pulupa/illustrations/ based on figure from [5].

the downstream shocked matter flows away with a smaller velocity v_d. In the lab system the upstream matter flows into the shock with velocity v_u and the downstream matter flows away with velocity $v_u - v_d$. We can calculate the energy of a particle crossing the shock by performing a Lorentz boost along the shock normal into the rest frame of the new region. For a particle initially in the upstream with velocity v_1 making an angle θ_1 with the shock normal its energy in the new frame of reference becomes

$$E' = \gamma E + \gamma(v_u - v_d)\cos\theta_1 p_1' = \gamma E + \gamma(v_u - v_d)\cos\theta_1 \gamma m v_1 \tag{2.7}$$

where $\gamma = 1/\sqrt{1 - ((v_u - v_d)\cos\theta_1)^2/c^2}$. Using $E = \gamma mc^2$ we then get

$$E' = \frac{E(1 + v_1(v_u - v_d)\cos\theta_1/c^2)}{\sqrt{1 - ((v_u - v_d)\cos\theta_1)^2/c^2}} \tag{2.8}$$

Moving back into the upstream we perform the inverse boost, giving final energy

$$E'' = E\frac{(1 + v_1(v_u - v_d)\cos\theta_1/c^2)}{\sqrt{1 - ((v_u - v_d)\cos\theta_1)^2/c^2}}\frac{\sqrt{1 - ((v_u - v_d)\cos\theta_1)^2/c^2}}{(1 + v_2(v_u - v_d)\cos\theta_2/c^2)} \tag{2.9}$$

For a particle having bounced across the shock n times the change in energy from making one additional pass is then

$$E_{n+1} = E_n\frac{1 + v_{n1}(v_u - v_d)\cos\theta_{n1}/c^2}{1 + v_{n2}(v_u - v_d)\cos\theta_{n2}/c^2} \tag{2.10}$$

All quantities are measured in the upstream restframe. By calculating the escape

probability and averaging over $\cos\theta$ it can be shown that the energy spectrum produced by such a process is [6]

$$N(E)dE = \frac{\gamma - 1}{E_0}\left(\frac{E}{E_0}\right)^{\gamma} dE \tag{2.11}$$

where γ is now the spectral index of the energy spectrum, found to be

$$\gamma = \frac{2v_d + v_u}{v_u - v_d} + \mathcal{O}\left(\frac{v_u - v_d}{c}\right) \tag{2.12}$$

The velocities v_u and v_d can be given in terms of the shock velocity v_s, the sound speed in the upstream region (Alfvén velocity) v_A, the average velocity of the downstream turbulences, v_T and the compression factor of the gas in the shock χ

$$v_u = v_s - v_A \tag{2.13}$$

$$v_d = \frac{v_s}{\chi} + v_T. \tag{2.14}$$

Combining (2.13), (2.14) with (2.12) gives

$$\gamma = \frac{(2+\chi) + \chi(2v_T/v_s - 1/M_A)}{(\chi - 1) - \chi(v_T/v_s + 1/M_A)} \tag{2.15}$$

M_A is the Alfvén mach number. A strong shock has a compression factor $\chi = 4$ and assuming $v_s \gg v_T$ we get $\gamma = 2$. The observed value should however be closer to 2.7 (see Eq. (2.5)). For $\chi = 4$ Eq. (2.15) gives $\gamma = 2.7$ if the ratio $v_T/v_s \approx 0.14$, alternately with $v_T = 0$ we get $\gamma = 4$ if the Alfvén mach number M_A is close to 7.

A more intuitive approach considers how momentum changes as a particle crosses the shock. The change in momentum of a particle crossing from the upstream into the downstream of the shock can be expressed as

$$p' = p + \Delta p \tag{2.16}$$

$$= p + \gamma m \Delta v \tag{2.17}$$

$$= p + \gamma m (v_u - v_d)\cos\theta \tag{2.18}$$

where the prime denotes momentum after transitioning the shock and θ is the angle between the particles momentum and the shock normal. The change in

energy is then

$$\Delta E = \int \frac{dp}{dt} dl = \int dp \cdot v \sim v\Delta p \tag{2.19}$$

$$= v\gamma m(v_u - v_d)\cos\theta \tag{2.20}$$

$$= Ev_1(v_u - v_d)\cos\theta/c^2 \tag{2.21}$$

where we use that $E = \gamma mc^2$. The result (2.21) is illuminating because it clearly shows that the increase in energy comes from the velocity difference between the upstream and downstream, $v_u - v_d$. The particle is stealing energy from the bulk motion of the shock. Furthermore, since the downstream is slower the change in energy is always positive. What happens when the particle is crossing the shock in the other direction, from the downstream into the upstream? The velocity difference is then $v_d - v_u$, which is negative and $\cos\theta \to -\cos\theta$ so the final result is once again positive. A point to note is that energy gain is independent of the shock parameters. While our model is simplistic, it shows that shock acceleration can produce the required power law spectrum and has been found capable of accelerating particles to traditional CR energies. Recent findings by the Fermi-LAT collaboration gives direct evidence for the acceleration of protons in SNRs by observing a characteristic pion-decay bump in gamma ray measurements of two supernova remnants [7].

2.2.3.2 Source Constraints

Energy A given process can obviously not accelerate particles to arbitrary energies. In terms of the energy required to sustain the galactic population of CRs we argued that SNRs are good candidates as acceleration sites (see section 2.2.2 In general, a given acceleration mechanism will have an energy threshold beyond which it is not effective. For diffusive shock acceleration this threshold is given by the finite lifetime of the shock, limiting the maximum number of cycles, and by the escape probability of the particles which increases with energy. Energy loss processes which increase with energy, such as synchrotron losses, will also at some point balance energy gain from crossing the shock. For acceleration in shocks this threshold is estimated to be around $E_{max} \approx 10^{12}$ eV to $E_{max} \approx 10^{17}$ eV [8]. This means that while the DSA mechanism may very well be responsible for acceleration of cosmic rays in the galaxy, suggesting SNRs as the typical galactic source, acceleration in some extragalactic sources and of CRs beyond the 10^{18} eV "ankle"

is still an open question.

Size Furthermore, regardless of the exact acceleration mechanism, any given source is subject to the geometric constraint that the particle has to fit inside the accelerator. Any type of statistical acceleration process requires a containment mechanism to keep the particles confined to the acceleration site. This containment comes in the form of a magnetic field B, and thus the size R_s of the source must be larger than orbit of the particle. The radius of orbit in a magnetic field for a charged particle is given by its Larmor radius $R_L = p/(ZeB)$. This allows us to construct a maximal energy based on known magnetic field strengths and source sizes. Taking into account the characteristic velocity of scattering centres βc we end up with the following requirement on source geometry

$$\left(\frac{B}{\mu G}\right)\left(\frac{R}{kpc}\right) > 2\left(\frac{E}{10^{18}\text{ eV}}\right)\left(\frac{1}{Z\beta}\right) \tag{2.22}$$

Using this relation one can construct so called "Hillas plots" as first done by Hillas in [9], showing what energies are attainable in accelerators of a certain size and with a certain magnetic field. From Figure 2.4 we then find that possible sites of acceleration for 10^{20} eV UHECRs are Active Galactive Nuclei (AGN), radio galaxies and pulsars.

2.2.3.3 Active Galactic Nuclei

In a normal galaxy the luminosity is purely the sum of all thermal emission from each of its stars. An active galaxy has substantial additional emissions which are not associated with any thermal process and is emitted from the galactic nucleus. The leading theory is that these emissions are due to mass accretion on the supermassive black hole (SMBH) in the center of the galaxy. The maximal energy gain from accretion onto the black hole will be $E_{max} \sim GmM/R_S$ where $R_s = 2GM/c^2$ is the Schwarzschild radius, giving $E_{max} \sim mc^2/2$. The luminosity which can be produced by accretion depends on how much energy is lost to the black hole. Models of the accretion process predict that the efficiency of the energy gain is about $\epsilon = 10\% - 20\%$, giving additional luminosity

$$L = \frac{\epsilon c^2 dm}{2dt} \tag{2.23}$$

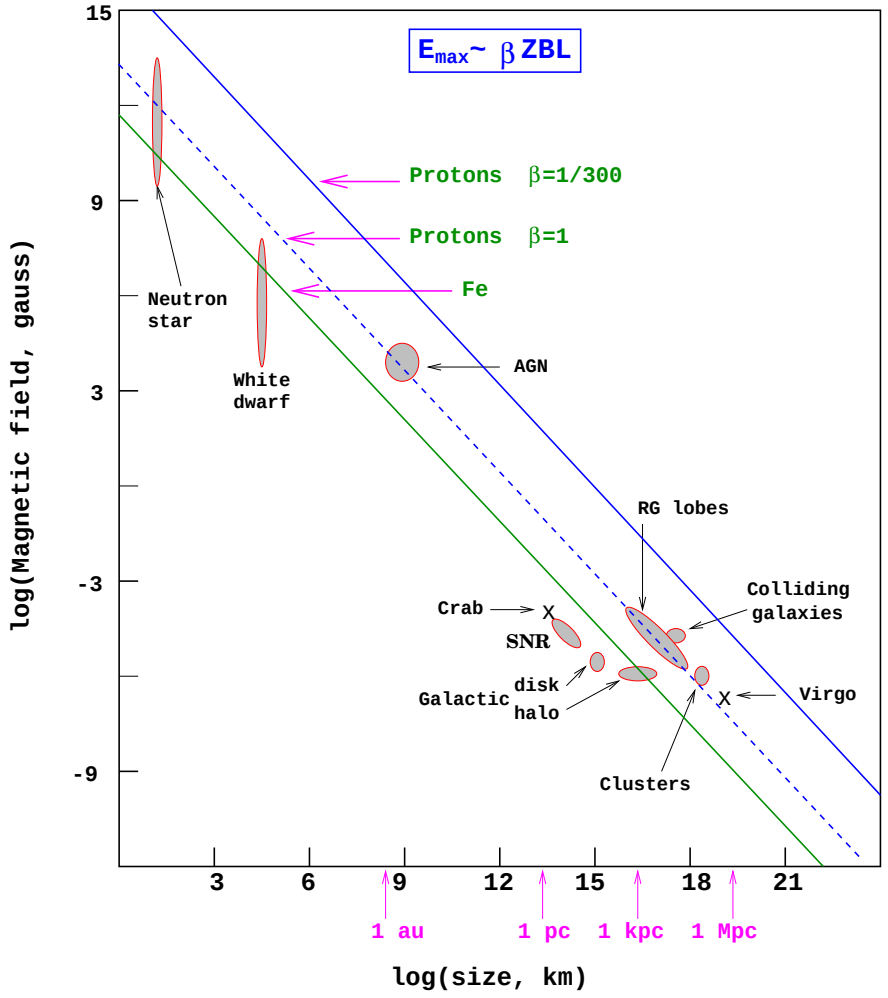

FIGURE 2.4: Hillas plot showing potential CR acceleration sites and their magnetic field strengths and sizes. Objects below the drawn lines can not accelerate protons or Fe nuclei to typical UHECR energies of 10^{20} eV . β is the characteristic velocity of the magnetic scattering centers [8].

on top of 'normal' thermal radiation. For mass consumption of $M_{\odot}$/yr and $\epsilon = 0.10$ we get a luminosity of $L \approx 3 \cdot 10^{45}$ erg/s. Many accretion disks also give rise to relativistic jets that emerge perpendicular to the disk and in both directions. Blazars are AGN where one of these jets point directly towards Earth and therefore appear as very luminous objects on the sky, making them very interesting candidates as UHECR sources.

Chapter 3

Gamma Rays

3.1 Gamma Ray production

It is an important distinction whether gamma rays are produced at the source or as secondaries during CR propagation. This is particularly true for extragalactic sources because high energy gamma rays are attenuated over cosmological distances. On such length scales the relevant medium of propagation is the cosmic microwave background (CMB) and the diffuse extragalactic background light (EBL). In the case where gamma rays are produced at the source this attenuation can result in very hard intrinsic spectral requirements for distant sources in order for model predictions to agree with observations. Since we assume that cosmic ray sources also produce gamma rays it becomes important to consider what portion of the observed gamma ray spectrum consists of secondary gamma rays. Essentially, we have two types of sources used in gamma ray models: The standard picture in which the source produces purely gamma rays, and an alternate picture in which the source produces cosmic rays with gamma rays forming entirely as secondaries from the propagation of these cosmic rays. Since very high energy (VHE) gamma rays are of particular interest due to their usefulness as 'messenger' particles we want to look specifically at which processes that can produce gamma rays of energies $E_\gamma = 10^8$ eV and above. The two relevant processes for production of gamma ray at this energy are inverse Compton scattering and pion photo-production.

3.1.1 Inverse Compton Scattering

Inverse Compton scattering is the process where a high energy electron collides with and transfers energy to a soft background photon

$$e^- + \gamma_b \rightarrow e^- + \gamma. \tag{3.1}$$

The obvious requirements for inverse Compton scattering to thrive is that there are high energy electrons and soft photons present at the production site. Without providing too much elaboration, typical sources will readily fulfil these requirements. In the presence of stars there will always be an abundance of soft photons produced by thermal emission, and electrons undergoing synchrotron acceleration will also radiate low energy photons. The presence of high energy electrons could also have several explanations. One possibility is a Blazar where electrons can be accelerated to high energies through diffusive shock acceleration inside the Blazar's jets. The presence of electrons in the jet will also inevitably produce low energy synchrotron photons, meaning inverse Compton scattering can happen. During propagation a background of soft photons exist in the form of the EBL and the CMB photons, and while primary VHE electrons will cool rapidly through synchrotron processes there can still be high energy electrons present throughout CR propagation as a result of pair production.

To describe a scattering process a useful quantity is the squared center-of-mass energy $s = (p_1 + p_2)^2 = (p_3 + p_4)^2$, which is a Lorentz invariant of the 2-particle scattering process $1 + 2 \rightarrow 3 + 4$ where p is the 4-momentum $p = (E, \mathbf{p})$.

In these terms the cross section for IC-scattering is given by

$$\sigma_{IC} = \begin{cases} \sigma_T(1 - s/m_e^2 + ...) & s/m_e^2 \ll 1 \\ \frac{3m_e^2}{4s}\sigma_T \left(\ln s/m_e^2 + \frac{1}{2} + ...\right) & s/m_e^2 \gg 1, \end{cases} \tag{3.2}$$

where σ_T is the Thomson cross section $\sigma_T = 8\pi\alpha^2/(3m_e^2)$. In the low energy limit this reduces to the non-relativistic Thomson process and for very high energies with $s \gg m_e^2$ IC-scattering is suppressed. To consider the energy gain of a photon due to IC scattering we look at a photon which has initial energy E_i in the lab frame and is hit by an ultra-relativistic electron with $\gamma \gg 1$. In the electron's frame of reference, denoted by a prime, the photon energy is given by $E_i' = E_i\gamma(1 - \beta\cos\theta)$ where θ is the collision angle between the electron and the photon, $\beta = v/c$. For

a low-energy photon with $E_i \ll m_e$ the energy change is given by [13]

$$E'_f \approx E'_i \left(1 - \frac{E'_i}{m_e}(1 - \cos\Theta)\right) \tag{3.3}$$

where Θ is the combined angle of deflection. Now in the lab frame the photon energy is found by another Lorentz boost $E_f = E'_i\gamma(1 + \beta\cos\phi)$. Thus the final energy of the photon in the lab frame is increased by a factor proportional to γ^2 except for an interval of unfortunate angles where the energy transfer is suppressed. On the average however, these angles are sparsely represented which means that IC scattering involving electrons with large γ can transfer a sizeable amount of energy to the photon in just one push. This makes IC scattering an effective way of producing high energy gamma rays.

3.1.2 Pion photo-production

The dominant hadronic process which produces VHE gamma rays is the decay of pions. Pions can be produced as a result of protons or nucleus interactions of the type

$$p + \text{nucleus} + ... \rightarrow p + \pi^{\pm} + \pi^0 + ... \tag{3.4}$$

where the produced pions decay as $\pi^0 \rightarrow 2\gamma$ and $\pi^{\pm} \rightarrow \mu\nu_\mu; \mu \rightarrow e\nu_\mu\nu_e$. Particularly neutral pion decay produces photons rapidly with the given decay channel responsible for 99% of decays and a mean lifetime of $8.4 \cdot 10^{-17}$ s. In the pion rest frame the two photons will be emitted in opposite directions with $\mathbf{p}_1 = -\mathbf{p}_2$ and each photon carrying energy $E_1 = E_2 = m_\pi/2$. If the pion is moving with some velocity v in the lab frame its energy will instead be given by a Lorentz transformation $E' = \gamma E(1+\beta\cos\theta)$ where θ is the angle between the outgoing photon and the incoming pion. Thus maximally energetic photons happen for $\cos\theta = 1$, when the photons are emitted along the direction of motion of the pion. For $E = m_\pi/2$ we get a maximal photon energy of

$$E_{max} = \frac{1}{2}\gamma(m_\pi + \beta m_\pi) = E_\pi(1 + \beta), \tag{3.5}$$

so in the ultra-relativistic limit $\beta \approx 1$ the maximal photon energy becomes $E = E_\pi$.

3.2 Energy loss processes

3.2.1 Pair production

The most dominant energy loss process for gamma rays is pair production of an electron/positron[1] pair on soft background photons, $\gamma + \gamma_b \to e^+ + e^-$. This is a threshold interaction which is active if the incoming high energy photon has sufficient energy to produce two electrons. The squared center of mass energy for particles 1 and 2 in the interaction $1 + 2 \to 3 + 4$ is

$$(p_1 + p_2)^2 = m_1^2 + m_2^2 + 2(E_1 E_2 - \mathbf{p}_1 \mathbf{p}_2) = m_1^2 + m_2^2 + 2E_1 E_2(1 - \beta_1 \beta_2 \cos\theta) \quad (3.6)$$

and similarly for end products 3 and 4. The threshold energy is given in the center of mass frame when end product electrons have zero momentum, that is when they are produced with the minimum possible energy $E = m_e$. In that case, for the interaction $\gamma + \gamma_b \to e^+ + e^-$, we get

$$s_{min} = 2E_\gamma \epsilon_b (1 - \cos\theta) = 4m_e^2. \quad (3.7)$$

By definition $\mathbf{p}_1 + \mathbf{p}_2 = 0$ in the center of mass frame, so $\cos\theta = -1$ and the threshold for the interaction is given by $4E_\gamma \epsilon_b = 4m_e^2$. Therefore only HE gamma rays with

$$E_\gamma \geq \frac{m_e^2}{\epsilon_b} \quad (3.8)$$

can initiate pair production on background photons. The pair production cross section is given by [14]:

$$\sigma_{PP} = \frac{3\sigma_T}{16}\left(1 - \beta^2\right)\left[(3 - \beta^4)\ln\left(\frac{1+\beta}{1-\beta}\right) - 2\beta(2 - \beta^2)\right] \quad (3.9)$$

where $\sigma_T = 8\pi\alpha^2/(3m_e^2)$ is the Thomson cross section and $\beta = \sqrt{1 - 4m_e^2/s}$. For $s = 4m_e^2$ we notice that $\beta = 0$ and this is indeed the velocity of the outgoing electron in the center of mass frame. A low energy limit is then found by expansion around $\beta = 0$ and gives $\sigma_{PP} \sim \beta$, while the high energy limit is found around $\beta = 1$ where $\sigma_{PP} \sim \beta \ln(x\beta - 1)\ln(\beta - 1)$.

[1] Often simply referred to as 'electrons'

3.3 Gamma Ray Spectrum

We consider first a strong CR source surrounded by a low-energy background photon gas which is opaque to the protons. This enables pion production of gamma rays as protons react with the photons in the gas, γ_g, through the process $p+\gamma_g \rightarrow \pi+X$, where the neutral or charged pion will decay into (amongst others) gamma rays as described in section 3.1.2. The most important processes involving gamma rays are at this point pair production and inverse Compton scattering

$$\gamma + \gamma_g \rightarrow e^+ + e^- \tag{3.10}$$

$$e + \gamma_g \rightarrow e' + \gamma', \tag{3.11}$$

the products of which will initiate electromagnetic cascades on the background photons. By considering the energy development of these cascades we can gain information about the spectral properties of the final gamma ray flux, particularly the spectral index γ of the spectral energy distribution (SED) which has the form $AE^{-\gamma}$ with A being some normalization constant. The full discussion is due to Berezinskii et. al [1], but is included for convenience.

3.3.1 One component photon background

We describe a cascade by the particle that carries away the most energy in an interaction, the leading particle. For high energies we can consider the cascade as a gradual deceleration of the leading particle through the cascade interactions, which produces low energy electrons. The high energy regime of the cascade is given by $E\epsilon/m_e^2 \gg 1$ where e is the energy of the cascading particle and ϵ is the energy of γ_g. In each interaction at such high energies the leading particle experiences a fractional energy loss which is approximately equal to

$$f \approx \frac{1}{\ln(2E\epsilon/m_e^2)}, \tag{3.12}$$

while for $E\epsilon/m_e^2 \sim 1$ we get for both processes $f \approx 0.5$ and for $E\epsilon/m_e^2 \ll 1$ inverse Compton scattering has

$$f \approx \frac{4E\epsilon}{3m_e^2}. \tag{3.13}$$

The energy at which protons are capable of producing pions in the gas is

$$E_p \sim m_\pi m_p/\epsilon \tag{3.14}$$

and the characteristic energy of the initial photon or electron is

$$\epsilon_0 \sim 0.1E_p = 0.1m_\pi m_p/\epsilon. \tag{3.15}$$

The threshold energy for pair production in the gas is

$$\epsilon_\gamma \sim m_e^2/\epsilon. \tag{3.16}$$

Above this energy, for $E > \epsilon_\gamma$ the produced photons do not escape the source due to the process $\gamma + \gamma_g \rightarrow e^+ + e^-$. The minimum energy of an electron produced in pair production is

$$\epsilon_e = \frac{\epsilon_\gamma}{2}. \tag{3.17}$$

No electrons will be created with an energy less than ϵ_e, but they will still interact with background photons in inverse Compton scattering. The energy of a Compton photon is $E'_\gamma = fE$ and so the maximum energy of a Compton photon produced by electrons of energy ϵ_e is

$$\epsilon_x = \frac{4\epsilon_e^2\epsilon}{3m_e^2} = \frac{\epsilon_\gamma}{3}. \tag{3.18}$$

Now we consider the energy evolution of the cascade, which has roughly three stages: $E\epsilon/m_e^2 \gg 1$, $E\epsilon/m_e^2 \sim 1$ and $E\epsilon/m_e^2 \ll 1$. At high energies when $E\epsilon/m_e^2 \gg 1$ the energy of the leading particle is above the characteristic energy ϵ_γ and pair production causes gradual energy loss where the leading particle loses a small fraction of its energy in each interaction given by fE. In this regime the leading particle is alternately a photon or an electron and from each interaction the low energy particle will begin a new cascade of initial energy fE. In the stage where $E\epsilon/m_e^2 \sim 1$ the energy is divided evenly in each interaction as $f \approx 0.5$, and particles are reproduced at equal energies until they arrive at the threshold $e = \epsilon_e$ where no new electrons are formed. At this point electrons will cool through $e + \gamma_g \rightarrow e' + \gamma'$ until they have no energy. The end result is that only photons leave the source, with a high-energy cut off at ϵ_γ.

If we call the number of cascade particles of a certain species which pass through a given energy $q_s(E)$ and attempt to describe its energy dependence we find that, in the case of electrons, for $E < \epsilon_e$, $q_e =$ constant as no new electrons are produced.

Above this energy the difference in number of leading electrons passing through energy E and $E + dE$ depends on how many new particles are produced in the interval $(E, E + dE)$. If dE'/E is the number of secondaries of energy E produced by a primary of particle E' this should be equal to

$$dq(E) = -q(E')dE'/E \tag{3.19}$$

with the minus because at higher energies there are fewer particles. If we approximate that f = constant then $fE' = E$ and the solution becomes $q(E) = A/E$ with A being some constant. Since the fraction of electrons is not a function of energy, this relation will also hold for them. Therefore we have

$$q_e = \begin{cases} A/E, & \text{if} E \geq \epsilon_e \\ q_0, & \text{if} E \leq \epsilon_e \end{cases} \tag{3.20}$$

Now to consider the photon spectrum. One electron decelerating from energy E_e to energy $E_e - dE_e$ will emit dE_e/E_γ photons with energy $E_\gamma = fE_e$ each. During the entire cascade the number of electrons that pass through energy E_e is given by $q_e(E_e)$ so the number of photons produced should follow

$$n_\gamma(E_\gamma) = q_e(E_e)\frac{dE_e}{E_\gamma}. \tag{3.21}$$

For energies above ϵ_γ the photons do not escape the source due to pair production, so $n_\gamma(E_\gamma) = 0$ for $E_\gamma > \epsilon_\gamma$. For $E_e < \epsilon_e$, when $q_e(E_e) = q_0$ and the average photon energy is that of fE_e with f given by Eq. (3.13), giving $E_\gamma = \frac{4}{3}E_e^2\epsilon/m_e^2$, we get from Eq. (3.21)

$$n_\gamma(E_\gamma) = AE^{-3/2}. \tag{3.22}$$

which is valid for $E_\gamma \leq \epsilon_x$, ϵ_x being the characteristic maximum energy of photons produced in from IC scattering when no more electrons are produced in the cascade. The final relevant energy regime is that of $\epsilon_x \leq E_\gamma \leq \epsilon_\gamma$, where electrons are produced but photons still escape the source. Here Eq. (3.20) says $q_e(E_e) = A/E$ and we approximate the electron energy with a power-law $E_e = kE_\gamma^m$ which from Eq. (3.21) then yields

$$n_\gamma(E_\gamma) = A'E_\gamma^{-2} \tag{3.23}$$

where A' is a constant. Since all electrons eventually pass on their energy to photons, the normalization constants A and A' can be computed from the condition that the total photon energy must be equal to the energy of the initial cascade

particle

$$\int_0^{\epsilon_\gamma} E_\gamma n_\gamma(E_\gamma) dE_\gamma = \epsilon_0, \tag{3.24}$$

The final result for the overall photon spectrum can then be combined in terms of (E_γ/ϵ_x):

$$n_\gamma(E_\gamma) = \begin{cases} (K/\epsilon_x)(E_\gamma/\epsilon_x)^{-3/2} & : E_\gamma \leq \epsilon_x, \\ (K/\epsilon_x)(E_\gamma/\epsilon_x)^{-2} & : \epsilon_x \leq E_\gamma \leq \epsilon_\gamma \\ 0 & : E_\gamma \geq \epsilon_\gamma \end{cases} \tag{3.25}$$

with $K = \epsilon_0/[\epsilon_x(2 + \ln 3)]$.

3.3.2 Two component photon background

For a background consisting of one population of photons γ_g with energy ϵ and density $n(\epsilon)$ and another populations of photons γ'_g with energy ϵ' and density $n(\epsilon')$ we must also account for the interactions of cascading particles with the second gas of photons. We consider the case where $\epsilon \ll \epsilon'$ and $n(\epsilon) \gg n(\epsilon')$. At the first stage of the cascade where $E > \epsilon_\gamma$ the development is not affected by the second photon population. As $n(\epsilon) \gg n(\epsilon')$ the interactions with the γ_g photons completely dominate this stage and there are no changes to $n_\gamma(E_\gamma)$. We call the one component produced spectrum from Eq. (3.25) $n^0_\gamma(E_\gamma)$ and consider it as $n_\gamma(E_\gamma)$ to the zeroth order in interactions with the second photon population. In the second stage, where pair production on γ_g photons stops as $E < \epsilon_\gamma$, the cascade will develop due to the interactions

$$\gamma + \gamma'_g \rightarrow e^+ + e^- \tag{3.26}$$

$$e + \gamma_g \rightarrow e' + \gamma' \tag{3.27}$$

that is, photons from the zeroth order spectrum will produce pairs with the γ'_g photons and electrons produced cool off by inverse Compton scattering. This becomes possible because the characteristic energy $\epsilon'_\gamma = m_e^2/\epsilon'$ is less than ϵ_γ when $\epsilon' \gg \epsilon$ and the cascade has a second interaction for pair production that picks up when the primary pair production interaction is below threshold. Thus all photons of the zeroth order spectrum with energy $E_\gamma \geq \epsilon'_\gamma$ transform into pairs. The minimum energy of an electron is one produced at threshold with

$E_{e,min} = \epsilon'_e = \epsilon'_\gamma/2$. A Compton photon produced will, as before, have the characteristic energy $\epsilon'_x = \frac{1}{3}\epsilon\epsilon'_\gamma/\epsilon'$.

To find $n_\gamma(E_\gamma)$ we first calculate the number of electrons generated by the zeroth order spectrum, $q_e(E_e)$ which describes the total number of electrons that passes through the energy E_e during the entire cascade. No electrons can be created with an energy less than $\epsilon'_e = \epsilon'_\gamma/2$, so for $E_e \leq \epsilon'_\gamma/2$ we clearly find that that $q_e(E_e) =$ constant. Above this energy, an increase in the number of electrons dq_e over an increase in energy dE happens due to pair production from n^0_γ photons. In terms of electron energy the photons carry approximately $E_\gamma = 2E_e$ and the change in number of electrons becomes

$$dq_e(E_e) = -2n^0_\gamma(2E_e)d(2E_e). \tag{3.28}$$

From Eq. (3.25) we then find that above $\epsilon'_\gamma/2$, $q_e(E_e)$ becomes

$$q_e(E_e) = 2\sqrt{2}K(E_e/\epsilon_x)^{-1/2} \tag{3.29}$$

which is valid up to the energy $E^c_e = f_e(\epsilon_x)\epsilon_x$ where $f_e(E_\gamma)$ is the fraction of the energy taken by the leading electron in the process $\gamma + \gamma'_g \to e^+ + e^-$. Here the spectrum of zeroth order photons goes as E^2_γ so

$$q_e(E_e) = K(E_e/\epsilon_x)^{-1}. \tag{3.30}$$

Combining to find the total photon spectrum from the cascade is now done from Eq. (3.21) for the different energy ranges and yields

$$n_\gamma(E_\gamma) = \begin{cases} (K/\epsilon'_x)(E_\gamma/\epsilon'_x)^{-3/2} & : E_\gamma \leq \epsilon'_x, \\ (K/\epsilon'_x)(E_\gamma/\epsilon'_x)^{-2} & : \epsilon'_x \leq E_\gamma \leq \epsilon'_\gamma \\ 0 & : E_\gamma \geq \epsilon'_\gamma \end{cases} \tag{3.31}$$

where now $K = \epsilon_0/[\epsilon'_x(2 + \ln 3\epsilon'/\epsilon)]$.

3.3.3 Arbitrary photon gas

For an arbitrary photon gas the resulting cascade spectrum is found in largely the same way. We consider a photon population where the density of the population decreases for higher energies. Then there will be some effective cut off where the

density of the population is no longer sufficient to absorb gamma rays by the process $\gamma + \gamma_g \rightarrow e^+ + e^-$. We call this high energy threshold ϵ_{max}. Similarly, there will be a very dense population of photons with some minimum energy ϵ_{min}. Following the same reasoning as before, we find that there are two characteristic energies associated with the problem:

$$\epsilon_\gamma = \frac{m_e^2}{\epsilon_{max}} \tag{3.32}$$

$$\epsilon_x = \frac{\epsilon_\gamma \epsilon_{min}}{3\epsilon_{max}}. \tag{3.33}$$

Above ϵ_γ pair production is effective and suppresses the entire gamma ray flux, giving

$$n_\gamma(E_\gamma) = 0 \text{ for } E_\gamma \geq \epsilon_\gamma. \tag{3.34}$$

Below the energy ϵ_x all photons produced are results of electrons cooling through IC scattering, and this gives a cascade spectrum

$$n_\gamma(E_\gamma) \sim E_\gamma^{-3/2} \text{ for } E_\gamma \leq \epsilon_x. \tag{3.35}$$

To determine what the spectrum should look like in the range $\epsilon_x < E_\gamma < \epsilon_\gamma$, consider a photon background with three components with energies ϵ_1, ϵ_2 and ϵ_3. Considered individually, the components at energies ϵ_1 and ϵ_3 would give a spectrum that changes in spectral index at energy $\epsilon_x = 1/3(\epsilon_1/\epsilon_3)\epsilon_\gamma$ from $\gamma = 1.5$ to $\gamma = 2.0$ while the components ϵ_2 and ϵ_3 would give the same spectral transition at $\epsilon'_x = 1/3(\epsilon_2/\epsilon_3)\epsilon_\gamma > \epsilon_x$. Therefore we can argue that in the region $\epsilon_x < E_\gamma < \epsilon'_x$ the spectrum will be steeper than $\gamma = 1.5$ with a transition towards $\gamma = 2.0$ at the energy ϵ'_x. If instead the distribution of background photons is continuous in energy, with higher energies being less populous, there should be a gradual steepening of the SED between ϵ_x and ϵ_γ with $n_\gamma(E_\gamma = \epsilon_x) \sim E_\gamma^{-1.5}$ that tends towards $n_\gamma(E_\gamma) \sim E^{-2.0}$ for higher energy, until is is cut off at $E_\gamma = \epsilon_\gamma$. In the case of very steep background spectra, this is essentially a two-component spectrum and yields a spectrum similar to $E^{-2.0}$ for $\epsilon_x \leq E_\gamma \leq \epsilon_\gamma$, essentially reproducing (3.31):

$$n_\gamma(E_\gamma) = \begin{cases} (K/\epsilon_x)(E_\gamma/\epsilon_x)^{-3/2} & : E_\gamma \leq \epsilon_x, \\ (K/\epsilon_x)(E_\gamma/\epsilon_x)^{-2} & : \epsilon_x \leq E_\gamma \leq \epsilon_\gamma \\ 0 & : E_\gamma \geq \epsilon_\gamma \end{cases} \tag{3.36}$$

where

$$\epsilon_\gamma = \frac{m_e^2}{(1+z)\epsilon_{max}}, \quad \epsilon_x = \frac{1}{3}\frac{m_e^2}{\epsilon_{max}^2}\epsilon_{min}. \tag{3.37}$$

Here we have also accounted for the fact that extragalactic sources can have significant red shift. It is worth mentioning that in a more detailed evaluation found in [18], the exponent for the region $\epsilon_x \leq E_\gamma \leq \epsilon_\gamma$ is found to expand as a series

$$\gamma = \frac{3}{2} + \frac{1}{4} + \frac{1}{8} + \frac{1}{16} \ldots \approx 2 \tag{3.38}$$

and the number of terms to be included depends on absorption probabilities for electrons and photons. An essential feature of the resulting power-law spectrum is that its features are independent of the distribution of the initial cascade particles. The characteristic energy of the initial particle, ϵ_0, only contributes to the overall normalization of the spectrum. Additionally, the shape of the background photon densities do not alter the behaviour of the spectrum below ϵ_x or above the cutoff, but will in general affect how rapidly the spectral index changes towards $\gamma = 2.0$ for energies above ϵ_x.

3.4 Photon backgrounds

The universe contains a series of background photon populations, an overview of which are presented in Figure 3.1.

From this we see that the two dominating photon backgrounds are the CMB and the EBL. The CMB as we know is assumed to be leftover thermal radiation from the big bang and has a near perfect black-body spectrum with a temperature of approximately $T = 2.7$ K, giving an average photon energy $\epsilon_{CMB} \simeq 3kT \approx 7 \cdot 10^{-4}$ eV. Additionally, with a number density of approximately $\mathcal{N}_{CMB} \approx 410$ cm^{-3} the energy density of the CMB photons becomes $u_{CMB} = 2.87 \cdot 10^{-1}$ eV/cm^{-3}. The second dominant background is the two component EBL which roughly consists of radiation emitted by stars and galaxies, as well as re-emission of this light by dust.

3.4.1 Extragalactic Background Light

The EBL is the resulting diffuse UV/optical radiation emitted by stars and galaxies, as well as infrared re-emission of this light by dust. The total energy of the EBL is then purely dependent on galaxy formations, but due to dust re-emission the energy is spread out over a broader spectrum. A strict lower limit on the

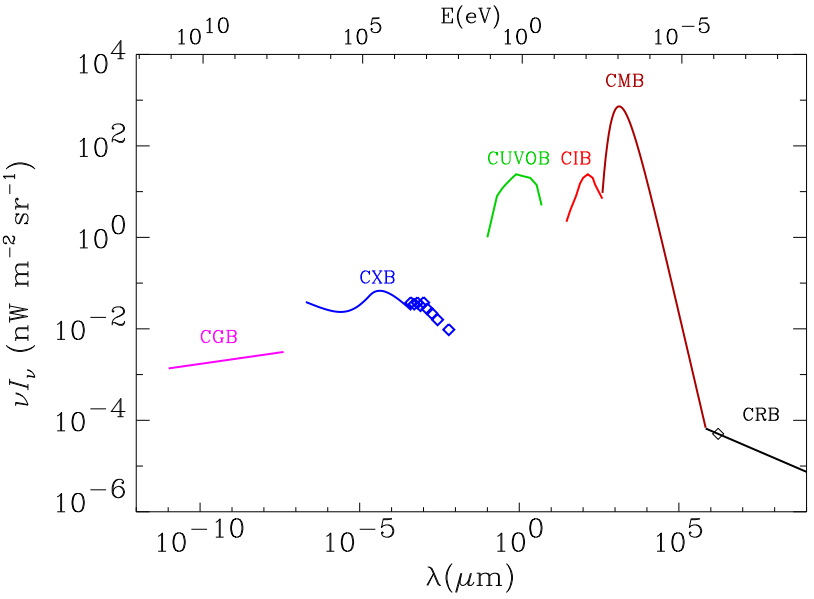

FIGURE 3.1: An overview of cosmic photon populations, the major components of which is the cosmic microwave background (CMB), the ultraviolet and optical background (CUVOB) and the infrared background (CIB). The latter two are more commonly referred to as the extragalactic background light (EBL) in this paper [10].

EBL comes simply from galaxy number counts and integrating their cumulative brightness, while an upper limit can be derived by considering the attenuation of VHE gamma rays due to pair production on soft photons [10]. This also implies that the EBL affects the observed spectrum from VHE gamma ray sources such as blazars, particularly in the energy range of $10^{10} - 10^{13}$ eV. As such, the intensity and spectrum of the EBL is of interest to calculate intrinsic blazar spectra in an energy regime where we wish to know more about particle acceleration mechanisms and VHE gamma ray production. On the other hand, knowledge of the intrinsic blazar spectra could be used to define limits on the EBL and its evolution.

Direct measurement of the EBL is generally difficult due to the presence of foreground light from our galaxy as well as the zodiacal light, but there exists a plethora of empirical modelling techniques. These can be roughly categorized into Backwards Evolution (BE) and Forward Evolution (FE) models. The EBL intensity is estimated by the total emission of all stars and galaxies integrated over

redshift. In the BE case the present epoch local galaxy population is extrapolated backwards in time, while in the FE case stars and galaxies are evolved from cosmological starting conditions to obtain spectral properties at any epoch. More advanced models also include formations of galaxies and their interactions, and obtain the EBL spectrum by matching parameters in universe evolution to agree with that of the observed local universe. A more detailed comparison of models can be found in [11] and the energy density of four commonly used models is presented in Figure 3.2. The high energy peak of the figure corresponds to the UV/optical galaxy light component, while the lower energy peak is the dust re-emission component with wavelengths in the IR. From the figure we find that the energy density of the EBL is of order $u_{EBL} \sim 10^{-3}$ eV/cm^3 which is significantly less than that of the CMB at $u_{CMB} = 2.87 \cdot 10^{-1}$ eV/cm^3. On the other hand, the EBL photon energies are much higher, with the average CMB photon having $\epsilon_{CMB} \approx 7 \cdot 10^{-4}$ eV while EBL photons range between $\epsilon_{EBL} \sim 10^{-3} - 10^{1}$ eV.

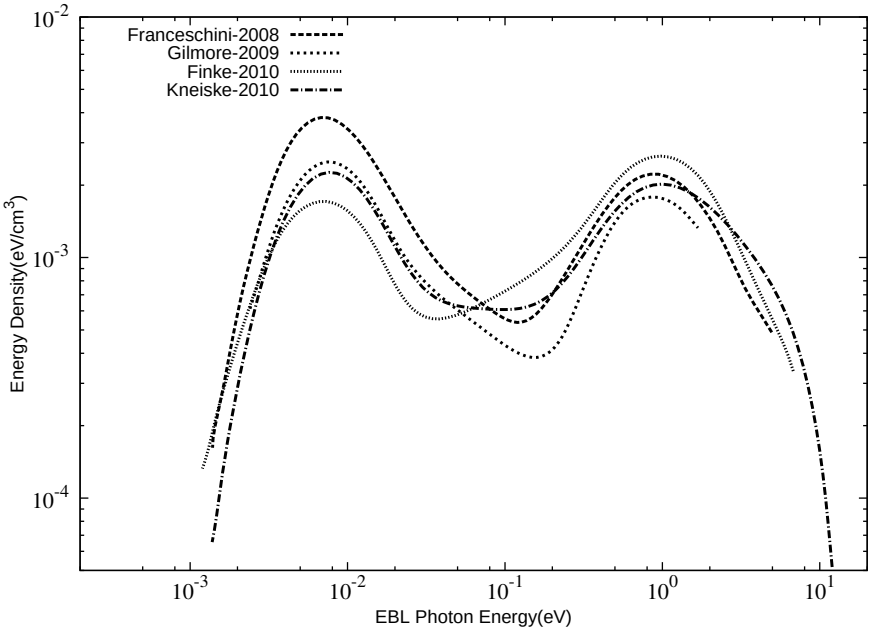

FIGURE 3.2: Comparison of EBL energy density predicted by various EBL models as a function of photon energy [11].

This means that the CMB and EBL agree well with the assumptions made in Section 3.3.2, with $n(\epsilon_{CMB}) \gg n(\epsilon_{EBL})$ and $\epsilon_{CMB} \ll \epsilon_{EBL}$. Moreover, while

the shape of the EBL is roughly comparable to a two component spectrum by itself, the combination of the CMB and EBL constitutes a "very steep background spectrum" as discussed in Section 3.3.3 and we expect that high energy gamma rays cascading on the CMB and EBL produce a spectrum with features given by Eq. (3.36) with

$$\epsilon_\gamma = \frac{m_e^2}{(1+z)\epsilon_{EBL}}, \quad \epsilon_x = \frac{1}{3}\frac{m_e^2}{\epsilon_{EBL}^2}\epsilon_{CMB}. \tag{3.39}$$

where ϵ_{EBL} is now the maximum energy of the EBL spectrum at $\epsilon_{EBL} \approx 10^1$ eV and adiabatic energy loss to the expansion of the universe has been included.

3.5 Effect of Extragalactic Magnetic Field

We have so far not considered the effects of the EGMF in any detail. The universe is thought to be pervaded by magnetic fields at all scales and the study of their generation, evolution and observational bounds is a wide field of research. The EGMF specifically points to the magnetic fields which exist between galaxies and are most commonly characterized by the mean magnetic field strength B and some coherence length λ_B. In the large scale structure of space the two most extensive regions are those of cosmic voids and galaxy filaments. Explained very briefly, the cosmic voids are vast regions of very low mean densities which consists of the space which is generally free of galaxy clusters. Galaxy filaments are the thin thread-like structures that form the boundaries of the cosmic voids. One often used model for the EGMF consists of magnetic field 'bubbles' with a size given by the coherence length and which contain a homogeneous field of strength B with a random alignment. In an even simpler case we divide space into cubes of length λ_B containing a magnetic field of some random alignment and strength B. One of the most fundamental issues with the EGMF is that no conclusive bound on either B or λ_B has been found. Furthermore, the field strength in voids are presumably much lower than field strengths inside filaments. Therefore in a 1D model of propagation through the EGMF we consider a certain fraction of space to consist of filaments where the magnetic field is much higher, and we populate the direction of travel with such filaments evenly. Current research suggests a variety of methods to determine bounds on the EGMF, and we will mention a few in passing. Upper bounds on the EGMF can be found through Faraday rotation measurements. Faraday rotation is the phenomenon where the polarization vector of a linearly polarized electromagnetic wave is rotated by some angle, $\Phi = RM\lambda^2$

where RM is the rotation measure which is connected to magnetic field strength. This gives an upper bound because observation of linearly polarized radio emission from distant quasars does not reveal any rotation of the polarization plane. Consideration of Faraday rotation data thus yields an upper bound

$$B \leq 2 \cdot 10^{-9} \frac{\lambda_B}{l_H} \tag{3.40}$$

where l_H is the horizon length [19]. Cosmic rays of ultra high energies have already been discussed (Sec. 2.1.1) and their origin is likely to be extragalactic sources. This means that UHECRs cross the EGMF when propagating towards earth. Charged particles are deflected by magnetic fields, and in the case of cosmic rays the deflection is given analytically by [8]

$$\theta(E,d) = 0.8^\circ q \left(\frac{E}{10^{20}\text{ eV}}\right)^{-1} \left(\frac{d}{10\text{ Mpc}}\right)^{1/2} \left(\frac{l_c}{1\text{ Mpc}}\right)^{1/2} \left(\frac{B}{10^{-9}\text{ G}}\right). \tag{3.41}$$

where the source distance $d \gtrsim l_c$ and qe is the charge of the particle. Thus the EGMF displaces the particle from the direction towards the source, allowing for the possibility of using CR measurements to determine the strength of the magnetic field. Finally, gamma ray observations can also be used in a number of ways to glean information about the EGMF. One method is to consider the delay of gamma ray arrival times as described in [20], but a more interesting method in light of our chosen topic is the suppression of gamma ray flux due to magnetic fields. The effect of the EGMF on gamma ray propagation is the deflection of electrons which form as a part of the cascade. Deflections will in principle scale as B/E_e, so for a fixed magnetic field strength there will be some value for E_e where the cascade begins to experience a notable decrease in electrons as they are thrown out of the observational cone. Particles are ejected from the source inside a cone of some opening angle θ_{jet}, as for instance in the case of a blazar. This defines some angular spread in which the resulting gamma rays are observable. For sufficiently high energies the deflection is too small to result in an observable loss of flux, but as the energy decreases electrons will be deflected significantly and the observer will experience a drop in flux. Finally, deflections become 'total' and the electrons are smeared out isotropically due to the random alignment of the magnetic field. Beyond this, there is no more flux reduction due to the magnetic field. Seen in light of our cascade theory, this suggests there is some critical energy $\epsilon_{B+}(B)$ for which the deflection becomes sufficient to throw electrons 'out of the cone'. At this point there will be a break from the spectrum predicted in Eq. (3.36) which will reform at some energy ϵ_{B-} where the deflections have become

isotropic. The difference in flux should then correspond to the subtended angle by the jet, $\Omega = 2\pi(1 - \cos\theta)$ sr, divided by the total solid angle 4π sr. The approach for utilizing gamma ray spectra to form bounds on the EGMF is to compare simulated spectra to the observational results. The effect of the magnetic field is to wash out part of the flux. Observations made in the lower energy regime by for instance Fermi-LAT gives an upper bound to the flux and thus allows a lower bound to be set on the EGMF: It must be sufficiently large to prevent the simulated flux from transgressing the observational limit. On the other hand, in the high energy range, gamma rays are detected by ACTs such as H.E.S.S and a limit is set on the EGMF so that it does not wash out this signal. This approach to find upper and lower limits on the EGMF has been pursued in for instance [21].

Chapter 4

Monte Carlo Simulations of Gamma Ray spectra

4.1 ELMAG

We are interested in comparing our analytical model for the general cascade features of observed gamma ray spectral energy distributions to that of spectra produced by sources. Notably, our model predicts that the resulting spectrum from an electromagnetic cascade is remarkably insensitive to source parameters. The typical source we wish to consider is a blazar and our method of doing so is through a simulation. To simulate blazar spectra we use the ELMAG software of Kachelrieß et. al which is available at `http://elmag.sourceforge.net/`. ELMAG is a Monte Carlo simulation program of electromagnetic cascades initiated by VHE gamma rays on the CMB and EBL backgrounds for a variety of EBL models and source parameters. As a gamma ray source ELMAG uses a power law distribution $dN/dE = E^{-\gamma}$ for some energy interval between E_{min} and E_{max}, generating photons through weighted sampling and then tracks the development of any electromagnetic cascades initiated by the primary gamma rays through pair production $\gamma + \gamma_b \to e^+ + e^-$ and inverse Compton scattering $e + \gamma_b \to \gamma + \gamma_b$, as well as deflections in extragalactic magnetic fields and synchrotron losses. ELMAG provides the particle energies, incident angle and time delay of cascade secondaries at redshift zero. This is presented as both a diffuse spectrum and the spectrum of photon inside the 95% area of the Fermi-LAT point spread function, and additionally spectra binned with respect to time delay and cumulative time delay

are provided within the 95-PSF area. The full manual for the ELMAG software is available in [12].

4.2 Interaction Rate

The interaction rates for electrons and photons can be computed knowing the cross section of the relevant interaction process $\sigma(s)$ and the photon background energy density and are therefore sensitive to the EBL model used. For photons the relevant interaction is pair production, which has an energy threshold and cross section given by Eqs. (3.8), (3.9) respectively.

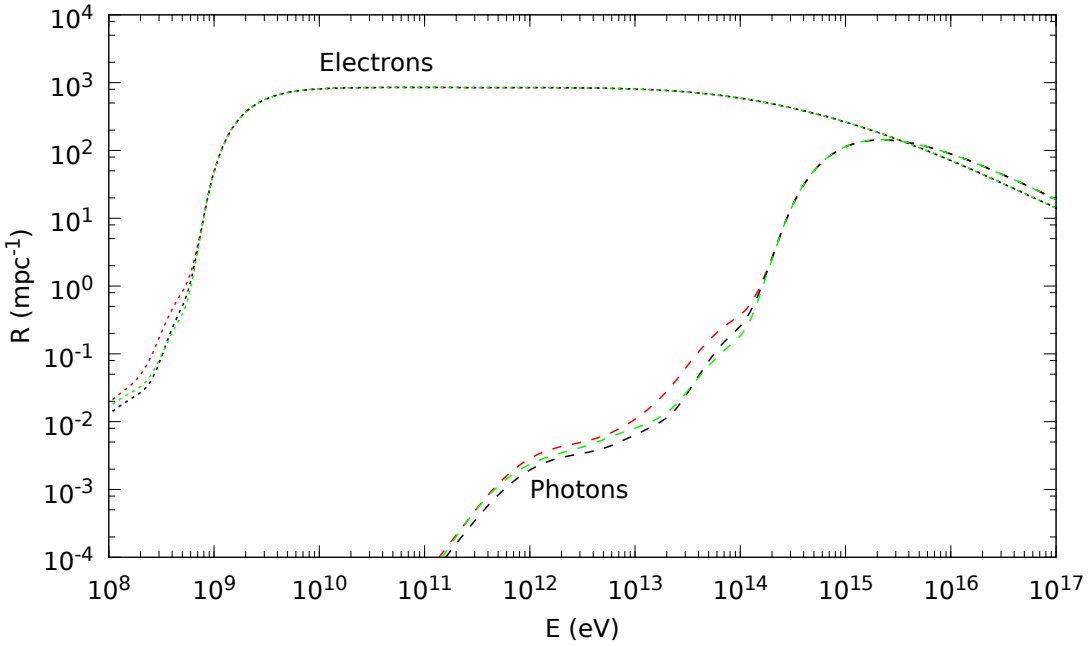

FIGURE 4.1: Interaction rates for electrons (upper short-dashed) and photons (lower dashed) at redshift $z = 0$. Incoming electrons and photons scatter on background photons, primarily the CMB and EBL, and shown are the number of interactions per megaparsec versus the incoming particle energy in eV for the EBL models of Kneiske et. al 'best-fit' (red) [15], Kneiske & Dole 'lower limit' (black) [16] and the model of Finke et. al (green) [17]. Comparison of these EBL models found in Figure 3.2.

4.2.1 Electrons

Figure 4.1 shows the interaction rate $R(E, z = 0)$ presented by the program for electrons and photons for some EBL models. The electron interaction rate is relatively featureless and approaches the Thomson regime for decreasing energy, as it should, but then becomes non-physical at $E \sim 10^{10}$ eV. This is a simulation feature designed to speed up calculations. In the Thomson regime photons carry away energies $E_\gamma \approx fE_e$ where f is given by Eq. (3.13) meaning that Compton photons are produced with energies

$$E_\gamma \approx 3.5 \cdot 10^9 \text{ eV} \cdot \left(\frac{E_e}{10^{12} \text{ eV}} \right) \tag{4.1}$$

which at $E_e \sim 10^{10}$ eV produces photons with energies $E_\gamma \sim 10^5$ eV, falling outside the interesting spectral region. Therefore some electron energy threshold is set to prevent the simulation from having to produce and track countless photons in the lower energy range. Instead, energy loss is calculated in a continuous energy loss approximation for electrons and fewer photons are produced.

4.2.2 Photons

The interaction rate for photons is best considered from higher energies towards lower. The first striking feature is the sudden drop in the interaction rate at roughly $E_\gamma \sim 10^{14}$ eV. This corresponds to the threshold value for pair production on CMB photons. The threshold energy, which is given by Eq. (3.8), yields $E_\gamma \geq 3.7 \cdot 10^{14}$ eV for pair production on CMB photons of average energy $\epsilon_{CMB} \approx 7 \cdot 10^{-4}$ eV. The second feature is the slight bump in the interaction rate which seem to indicate a new cut-off somewhere near $E_\gamma \sim 10^{13}$ eV. This would be due to interactions on the infrared bump of the EBL at $\epsilon_{EBL,IR} \approx 10^{-2}$ eV through the mechanism developed in Section 3.3.2 which predicts a component-wise cut off from the IR bump at $E_\gamma \approx 10^{13}$ eV. We see here that photons below the CMB pair production threshold continue to interact with the EBL, but the rate of EBL interactions is reduced by several orders of magnitude owing to the much larger density of the CMB. As is evident from Figure 3.2 the second high energy bump of the EBL at $\epsilon_{EBL,UV/OP} \approx 1$ eV should maintain the interaction rate beyond this until the final cut off at $E_\gamma = m_e^2/\epsilon_{EBL} \approx 10^{11}$ eV and this is clearly shown in the figure.

4.2.3 EBL dependency

Finally, we wish to consider the implication of different EBL models on the interaction rate. For electrons there are no energy thresholds to observe and analytically one expects EBL variations to be unimportant as electrons will instead interact exclusively with the much denser CMB. This is indeed observed, differences in the electron interaction rate are not noticeable except for low energies where $R(E_e, z)$ becomes non-physical. The same principle evidently holds true for photon interactions above the $3.7 \cdot 10^{14}$ eV CMB threshold, and only below this are we able to observe slight variations in the photon interaction rate between the different models. While differences in the rate at which photons produce electrons can very well accumulate into noticeable differences in the energy distribution of observed photons, these are too slight to comment on any variances in the characteristic energies used to predict spectral features, and consequently spectral features predicted in Section 3.3 should be reasonably well behaved irrespective of the chosen EBL model.

4.3 Cascade Spectra from Gamma Ray sources

4.3.1 Cascade spectra from sources at varying redshift

We begin by considering the diffuse gamma ray spectra from sources at three different redshifts for a single EBL model with constant primary particle energy $\epsilon_0 = 10^{14}$ eV and no magnetic field. The source in this case is similar to a blazar and consists of a jet with an opening angle $\theta_{jet} = 6°$, but the intrinsic spectra is constant $dN/dE = \epsilon_0$ instead of the expected power-law behaviour for blazars. We also consider briefly what effect changing the injection energy has on the resulting observed diffuse spectrum.

From looking at Figure 4.2, clearly the value of ϵ_0 has no effect on the resulting cascade spectrum once normalized[1]. Calculating the characteristic energies given by Eq. (3.37) yields $\epsilon_\gamma = 2.3 \cdot 10^{11}$ eV using $\epsilon_{EBL} = 1$ eV and $\epsilon_x = 6.1 \cdot 10^7$ eV with $\epsilon_{CMB} = 7 \cdot 10^{-4}$ eV. We see from the figure that the photon spectrum deviates from the $E^{-1.5}$ trendline at around 10^7 eV and begins to curve smoothly towards $E^{-1.9}$

[1]There is one obvious caveat here, ϵ_0 naturally has to be above the threshold for pair production or nothing will happen.

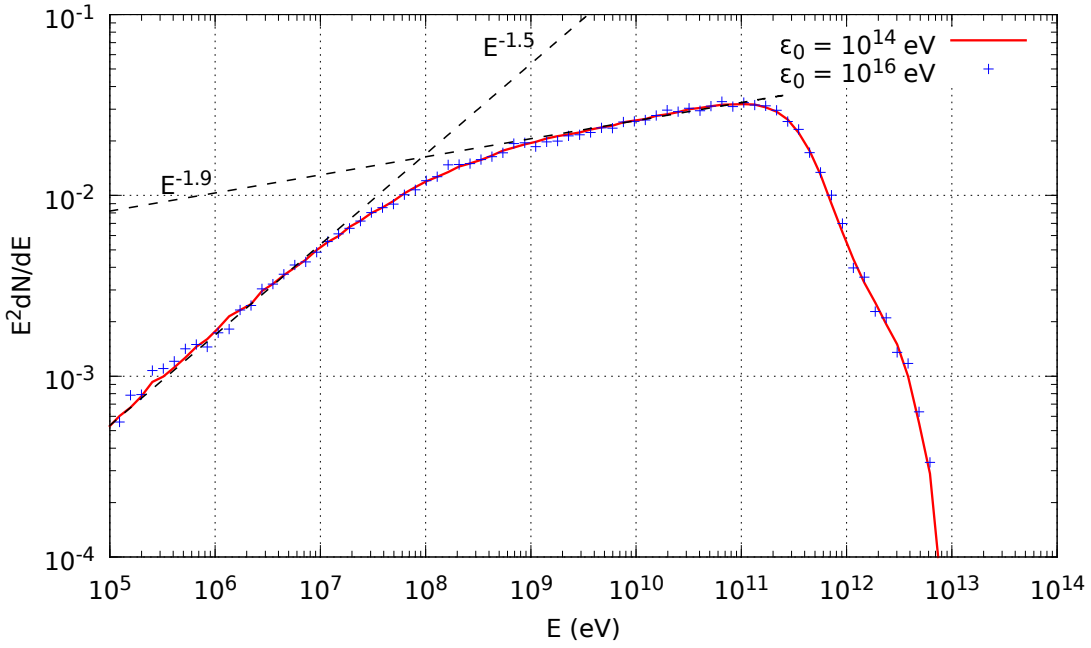

FIGURE 4.2: Normalized spectral energy distribution of the diffuse photon flux as predicted by a Monte Carlo simulation. Photons are injected at constant energy ϵ_0 from a source at redshift $z = 0.14$ with opening angle $\theta_{jet} = 6°$, and consequently initiate electromagnetic cascades on background photons modelled by the 'best-fit' model of [15].

for increasing energies. Finally there is an exponential decline in flux which begins just beyond 10^{11} eV where the spectrum breaks away from the $E^{-1.9}$ trendline.

In Figure 4.3 the normalized spectral density has been plotted for sources at three different redshifts, but with the same opening angle $\theta_{jet} = 6°$ and the same value for $\epsilon_0 = 10^{14}$ eV as well as the same EBL model and zero magnetic field. The cut off energy is dependent on the redshift, and we therefore predict analytically three different values for the cut off, namely $\epsilon_{\gamma,0.05} = 2.5 \cdot 10^{11}$ eV, $\epsilon_{\gamma,0.14} = 2.3 \cdot 10^{11}$ eV and $\epsilon_{\gamma,0.05} = 1.8 \cdot 10^{11}$ eV From the spectra presented in the figure, the ordering of the cut off energies do follow the predicted pattern, with lower cut off for higher redshift sources, but it would be imprudent to claim a better accuracy than to say the cut off from the figure is somewhere near $\epsilon_\gamma \approx 10^{11}$ eV for all redshifts. The break in the spectrum is however not redshift dependent in the analytical model and should occur for $\epsilon_x = 6.1 \cdot 10^7$ eV for all three spectra. From the figure we find that the spectrum deviates from its $E^{-1.5}$ behaviour at $E_\gamma \approx 10^7$ eV, but the tendency to follow the predicted $dN/dE \sim E^{-2}$ varies for the different redshifts. First of all, the spectral index indicated by the simulation is closer to $\gamma = 1.9$

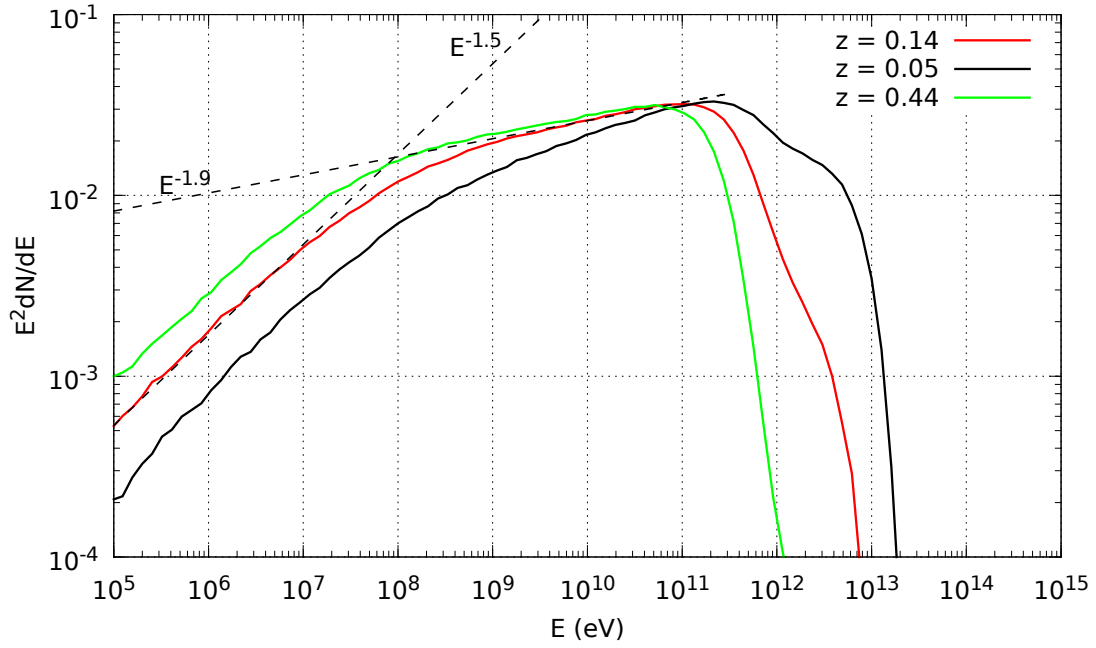

FIGURE 4.3: Normalized spectral energy distribution of the diffuse photon flux for sources at three redshifts. Photons are ejected from the source inside an opening angle $\theta_{jet} = 6°$ with initial energy $\epsilon_0 = 10^{14}$ eV, using the 'best-fit' EBL model of [15].

for the 'plateu' region between ϵ_x and ϵ_γ, 10^7 eV $\leq E_\gamma \leq 10^{11}$ eV. One possible improvement to this fit could be that not too many terms from Eq. (3.38) can be included. Secondly the tendency to curve towards $E^{-2.0}$ varies with redshift, higher redshift sources seem to approach the analytic limit more rapidly than lower redshift sources. Thus the plateau size is redshift dependent in the simulation model but not in the analytical case. Finally, the form of the exponential cut off varies with redshift, more distant sources have a sharper and less featured cut off at ϵ_γ.

4.3.2 Cascade dependency on EBL model

To consider the impact of varying EBL models on the observed spectra we shall briefly consider the results in Figure 4.4. Our analytical model of the spectrum only includes the EBL in terms of the maximal energy value ϵ_{EBL} and in the discussion of the spectral shape for energies $\epsilon_x \leq E_\gamma \leq \epsilon_\gamma$ as presented in Sec. 3.3.3. From Figure 3.2 we note that no two models have any significant shift in

the values for ϵ_{EBL} and as such the characteristic energies ϵ_x and ϵ_γ should not vary. Additionally, to first approximation, all EBL models essentially yield a two component EBL with little variance in distributed energy density and as such should not affect the $E^{-1.5} \rightarrow E^2$ changeover according to theory. From Figure 4.4 we see that the only noticeable difference in the spectra are beyond the ϵ_γ cut off, where the analytic model makes no further prediction than some form of exponential decay in flux.

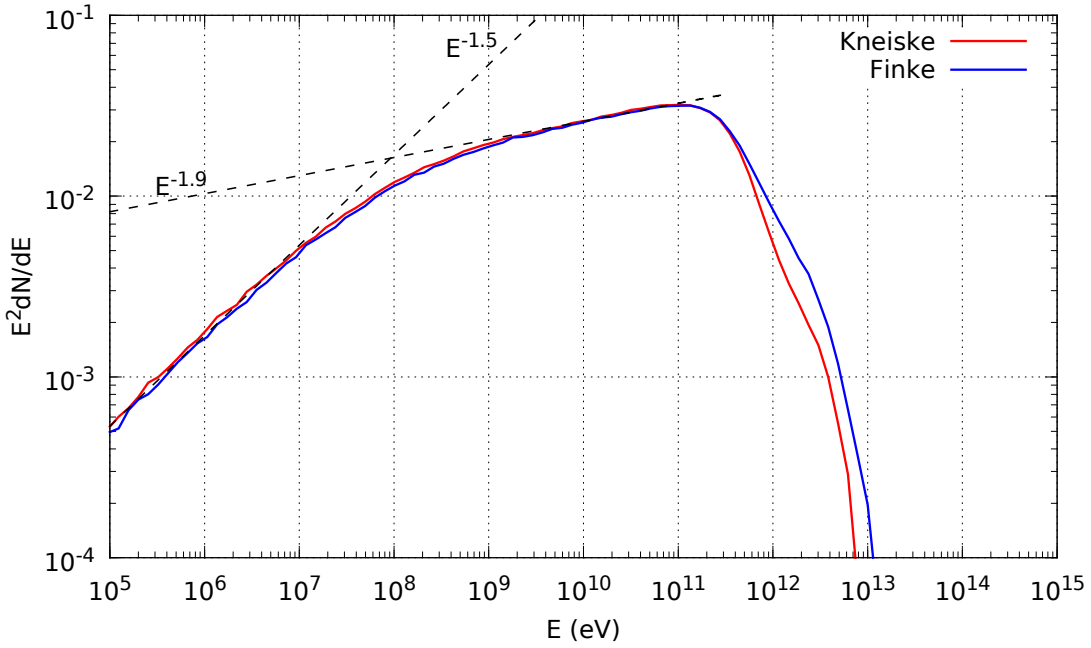

FIGURE 4.4: Normalized gamma ray spectra for a single source configuration using two different EBL models. The source is set at redshift $z = 0.14$ to eject primary photons of energy $\epsilon_0 = 10^{14}$ eV inside an opening angle of $\theta_{jet} = 6°$.

4.3.3 Cascade spectra for varying EGMF

In Figure 4.5 we have plotted cascade spectra for changing magnetic field strengths in simulation units. We observe immediately that applying a magnetic field has clear effects on the cascade spectra: Best considered from higher energies towards lower, comparing with the $B = 0$ G (red) spectrum, we see the magnetic field has no effect above some energy $\epsilon_{B+} \approx 10^{10}$ eV but then causes a sharp cut in the flux which seems to also follow a power law. This carries on until some other energy $\epsilon_{B-} \approx 10^8$ eV where the spectrum reforms. We can not analytically predict the

values for $\epsilon_{B\pm}$ with our current theory, however we do expect the flux reduction to be of order $4\pi/\Omega$ where Ω is the solid angle subtended by the source jet. This gives a magnetic flux-loss factor $k \approx 4 \cdot 10^2$. However, comparison in the low energy limit where all spectra reform to $dN/dE \sim E^{-1.5}$ we find that the multiplicative loss of flux is closer to $2 \cdot 10^1 \approx \sqrt{4\pi/\Omega}$.

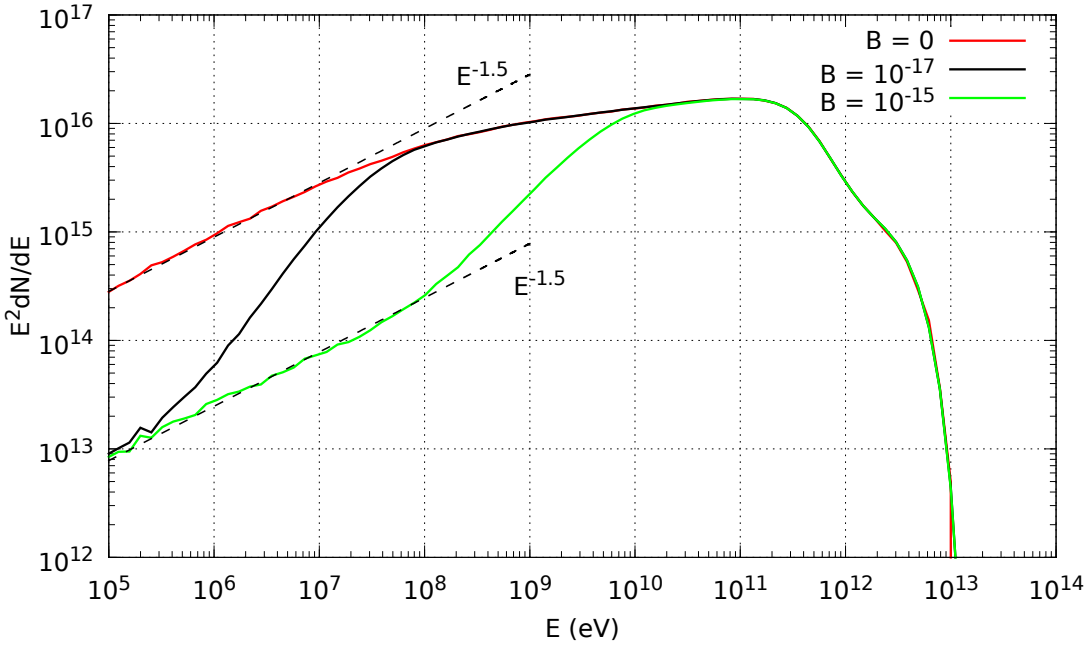

FIGURE 4.5: Cascade spectra plotted for changing EGMF strength. The EGMF is characterized by strength B in units of G with coherence length $\lambda_B = 1$ Mpc. The source at redshift $z = 0.14$ ejects gamma rays with constant energy $\epsilon_0 = 10^{14}$ eV within an opening angle $\theta_{jet} = 6^\circ$

Chapter 5

Conclusion

In this thesis we have considered an analytical model for the energy dependence of electromagnetic cascade spectra formed by very high energy gamma rays initiating cascades on the extragalactic background light. More specifically, we have reviewed essential theory on the topics of cosmic rays and gamma rays such as their composition, relevant energy loss processes and their behaviour in magnetic fields. In particular we have considered the cosmic ray relationship with gamma rays, such as the various mechanisms in which cosmic rays can interact with and produce gamma rays. Relevant questions in regards to this are which mechanisms are effective at producing gamma rays at the highest energies and how these high energy gamma rays propagate through the universe. Finally, we have compared the analytic cascade model with results from a Monte Carlo simulation that simulates such cascades initiated by very high energy gamma rays.

An electromagnetic cascade develops essentially through pair production and inverse Compton scattering

$$\gamma + \gamma_b \rightarrow e^+ + e^- \tag{5.1}$$

$$e + \gamma_b \rightarrow \gamma + e' \tag{5.2}$$

which means that the initiation of a cascade is a threshold reaction described by two characteristic energies, namely the threshold energy for pair production $\epsilon_\gamma = m_e^2 \epsilon_{EBL}^{-1}(1+z)^{-1}$ and the energy of Compton photons produced by electrons resulting from threshold pair production $\epsilon_x = (1/3) m_e^2 \epsilon_{CMB} \epsilon_{EBL}^{-2}$. The combined

result for the analytical model is given by Eq. (3.36) but is stated here for convenience:

$$n_\gamma(E_\gamma) = \begin{cases} (K/\epsilon_x)(E_\gamma/\epsilon_x)^{-3/2} & : E_\gamma \leq \epsilon_x, \\ (K/\epsilon_x)(E_\gamma/\epsilon_x)^{-2} & : \epsilon_x \leq E_\gamma \leq \epsilon_\gamma \\ 0 & : E_\gamma \geq \epsilon_\gamma \end{cases} \tag{5.3}$$

where K is some constant. We then proceeded to test our model predictions against spectra produced in a detailed Monte Carlo simulation using the ELMAG software. The results of these simulations are found in the figures of Section 4.3 along with analytical predictions for each case in the corresponding subsection, but we will discuss the compatibility of the analytical case and simulated case here. In Figure 4.2 we see that the change in injection energy ϵ_0 has no effect on the resulting cascade whatsoever. This is not surprising because at energies even only slightly above threshold, pair production becomes very effective and photons cool rapidly. The effect of injecting higher energy photons then simply reduces to a larger overall normalization since more energy is presented to the cascade. However, simulated spectra need to be fitted to observational data in any case and this is therefore inconsequential. One interesting consequence of this is that the spectrum formed in the cascade therefore becomes independent of the spectral index of the source. The energy distribution of gamma rays above threshold will have no effect on the shape of the cascade, and only contributes to its overall luminosity. However, to state the obvious, direct observation of a gamma ray source naturally sees both the cascade spectrum and any photons from the source which did not enter the cascade, i.e photons with energies below the pair production threshold and here the initial power law distribution contributes also to the shape of the observed spectrum.

The redshift of the source does alter the shape of the cascade spectrum, evident from Figure 4.3. The obvious way this happens is due to the adiabatic energy loss induced by the expansion of the universe, which comes into play as a factor of $1/(z+1)$ in the threshold energy. The not so obvious effect of increased redshift is that it makes the spectra look 'nicer' in accordance to our model. Specifically, in the energy region $\epsilon_x \leq E_\gamma \leq \epsilon_\gamma$ the spectrum approaches the predicted E^{-2} behaviour more rapidly for higher redshifted sources. In the case of a source at $z = 0.05$ the E^{-2} plateau is almost entirely suppressed. One possibility could be that for 'nearby' sources at low redshift the cascade does not fully develop. However, all photons in the cascade are Compton photons and this allows us to calculate the energy of the leading electron which transferred energy to them from the fractional energy loss in IC scattering, $E_c = fE_e$ where f is given by Eq. (3.13). For the $\epsilon_x \leq$

$E_\gamma \leq \epsilon_\gamma$ this yields electron energies of order $10^{11} - 10^{12}$ eV and this corresponds to an interaction rate for electrons of $R_e(E) \sim 10^3$ (Figure 4.1). Thus the interaction length for electrons is $\sim$ 1 kpc while even redshift $z = 0.05$ corresponds to a comoving distance of as much as $\sim$ 200 Mpc. This effectively kills the hypothesis that the cascade is simply underdeveloped. Another possible explanation could be that our assumption that the EBL and CMB constitute a "sharp" spectrum, thus essentially reducible to a two-component spectrum simply does not hold. As argued in Sec. 3.3.3 the tendency for the spectrum to curve towards E^{-2} depends on the shape of the arbitrary photon background. As explained in [22], a simple z-dependent scaling factor is not sufficient to accurately describe different sources because the EBL varies strongly in both total power and spectral energy distribution for different redshift. It is also explained that gammas from higher redshift sources are more strongly attenuated which could very well explain the sharper cut-off above threshold seen in Figure 4.3 for $z = 0.44$.

The dependency of the cascade spectrum on the EBL was also not observable within the regions where our analytical model makes predictions. In fact, the EBL seemed to only affect the shape of the exponential decay in flux for energies above the pair production threshold. While this is understandable, since the cut off energy is dependent on ϵ_{EBL}, it is also somewhat unfortunate that our model does not consider the shape of the EBL in more detail. This would naturally require a much more thorough analytical presentation, but the exact details of the EBL are of great interest because it allows us to learn more about the properties of gamma ray sources as discussed in Sec. 3.4.1 and in [10]. The analytical model for cascade spectra exhibits great generality and is remarkably insensitive, but this also reduces its predictive power. The same argument applies to the effect of magnetic fields, since we do not predict the values of $\epsilon_{B\pm}$ in our model, we can not connect cascade spectra to the values of B directly[1]. This is the most notable limitation to our model, while it predicts the overall features of the cascade spectrum to good accuracy we would very much like to connect it directly to the shape and size of the EBL and EGMF.

As a final concluding remark, the agreement between simulation models such as ELMAG and the analytical model of Berezinskii et. al is well established. The spectrum of an electromagnetic cascade initiated by a high energy gamma ray is indeed described most generally by the broken power law of Eq. (3.36) with characteristic energies ϵ_x and ϵ_γ found in Eq. (3.37). The general shape of the

[1]This would probably be a lot less troublesome to implement than any direct connection to EBL densities, however.

spectrum holds even with modifications to source redshift and the addition of an EGMF, where the effect of the latter is to induce an additional break in the spectrum over some energy interval $\epsilon_{B-} \leq E_\gamma \leq \epsilon_{B+}$.

Bibliography

[1] Berezinskii, V. S., and V. L. Ginzburg. *Astrophysics of Cosmic Rays.* Amsterdam: North-Holland, 1990. Print.

[2] L. O'C. Drury, Astropart. Phys. **39-40**, 52 (2012) [arXiv:1203.3681 [astro-ph.HE]].

[3] A. W. Strong, T. A. Porter, S. W. Digel, G. Johannesson, P. Martin, I. V. Moskalenko and E. J. Murphy, Astrophys. J. **722**, L58 (2010) [arXiv:1008.4330 [astro-ph.HE]].

[4] Khokhlov, A., Mueller, E., & Hoeflich, P. 1993, A & A, 270, 223

[5] Lee, M. A. 2000, Acceleration and Transport of Energetic Particles Observed in the Heliosphere, 528, 3

[6] A. R. Bell, Mon. Not. Roy. Astron. Soc. **182**, 147 (1978).

[7] M. Ackermann *et al.* [Fermi-LAT Collaboration], Science **339**, 807 (2013) [arXiv:1302.3307 [astro-ph.HE]].

[8] P. Bhattacharjee and G. Sigl, Phys. Rept. **327**, 109 (2000) [astro-ph/9811011].

[9] A. M. Hillas, Ann. Rev. Astron. Astrophys. **22**, 425 (1984).

[10] M. G. Hauser and E. Dwek, Ann. Rev. Astron. Astrophys. **39**, 249 (2001) [astro-ph/0105539].

[11] K. K. Singh, S. Sahayanathan, A. K. Tickoo and N. Bhatt, New Astron. **27**, 34 (2014) [arXiv:1310.8386 [astro-ph.HE]].

[12] M. Kachelriess, S. Ostapchenko and R. Tomas, Comput. Phys. Commun. **183**, 1036 (2012) [arXiv:1106.5508 [astro-ph.HE]].

[13] Vietri, M. (2008). *Foundations of high-energy astrophysics*. Chicago: University of Chicago Press.

[14] S. Lee, Phys. Rev. D **58**, 043004 (1998) [astro-ph/9604098].

[15] T. M. Kneiske, T. Bretz, K. Mannheim and D. H. Hartmann, Astron. Astrophys. **413**, 807 (2004) [astro-ph/0309141].

[16] T. M. Kneiske and H. Dole, arXiv:1001.2132 [astro-ph.CO].

[17] J. D. Finke, S. Razzaque and C. D. Dermer, Astrophys. J. **712**, 238 (2010) [arXiv:0905.1115 [astro-ph.HE]].

[18] V. S. Berezinsky and A. Y. .Smirnov, Astrophys. Space Sci. **32**, 461 (1975).

[19] R. Durrer and A. Neronov, Astron. Astrophys. Rev. **21**, 62 (2013) [arXiv:1303.7121 [astro-ph.CO]].

[20] A. Neronov, D. Semikoz, M. Kachelriess, S. Ostapchenko and A. Elyiv, Astrophys. J. **719**, L130 (2010) [arXiv:1002.4981 [astro-ph.HE]].

[21] W. Essey, S. 'i. Ando and A. Kusenko, Astropart. Phys. **35**, 135 (2011) [arXiv:1012.5313 [astro-ph.HE]].

[22] R. C. Gilmore, R. S. Somerville, J. R. Primack and A. Dominguez, arXiv:1104.0671 [astro-ph.CO].